
Article:
Kylafis, GF, Sleigh, PA, Tomlin, AS orcid.org/0000-0001-6621-9492 et al. (1 more author) (2019) Evacuation characteristics of released airborne TiO2 nanomaterial particles under different ventilation rates in a confined environment. Journal of Environmental Management, 233. pp. 417-426. ISSN 0301-4797

https://doi.org/10.1016/j.jenvman.2018.12.063

Evacuation characteristics of released airborne TiO_2 nanomaterial particles under different ventilation rates in a confined environment.

Georgios F. Kylafis[a], P. Andrew Sleigh[b], Alison S. Tomlin[a], Yaobo Ding[c,d]

[a] School of Chemical and Process Engineering, University of Leeds, LS2 9JT, UK

[b] Institute of Public Health and Environmental Engineering (iPHEE), School of Civil Engineering, University of Leeds, LS2 9JT, UK

[c] Institute of Lung Biology and Disease, Helmholtz Zentrum München, 85764 Neuherberg, Germany

[d] Comprehensive Pneumology Center-Member of the German Center for Lung Research (DZL), 81377 Munich, Germany

Abstract

A specially designed 32 m^3 airtight chamber that allows the implementation of various ventilation strategies was utilised to study the evacuation characteristics of airborne sub-micron particles generated from TiO_2 nanopowder in a potential indoor accidental release situation. Following the release using a heated line from a nebuliser system, the spatial and temporal variations in particle number concentration were recorded by three condensation particle counters (CPCs) distributed at specific locations in the chamber. A differential mobility spectrometer was co-located with one of the CPCs for the measurement of particle size distributions (PSDs). The different modal groups present within the measured PSDs were determined through a $\log_{10}$-normal fitting program. Of the ventilation rates evaluated, the greatest relative improvement in particle concentration and clearance time occurred at the highest rate (12 air changes per hour, ACH). At the same time, indications of cross-contamination from regions with strong mixing conditions to regions where mixing was poor, were obtained showing that the latter could operate as particle traps where localised poor ventilation might occur. However, reducing the ventilation rate led to: i) an increase of leftover particles in the air of the chamber when the cleaning process had been completed, and more specifically to an increased ratio of ultrafine particles over fine ones, resulting in the potentially dangerous accumulation of contaminants with high exposure hazards, ii) a decrease in ventilation efficiency, which at low evacuation rates became independent of distance from the inlet diffuser, iii) slower clearance of resuspended particles, with the lowest efficiency at the moderate ventilation rate.

Keywords: Engineered nanomaterials, exposure chamber, air quality, nanosafety, ventilation

1. Introduction

The acceleration of the manufacture and use of engineered nanomaterials (ENM) has led to an increase in the probability of the accidental release of sub-micron particles with varied size into the air and the concern that these will have possibly harmful health effects in humans. Emissions of particulate matter in nanotechnology workplaces where large amounts of ENM are involved, especially in the form of nanopowders, have been shown under normal operating conditions to be very limited (Kuhlbusch et al., 2011; Walser et al., 2012; Wang et al., 2011). However, processes like bagging, packaging, or cleaning of process equipment can significantly increase particle indoor concentrations and consequently the exposure of workers to various risks (Kuhlbusch et al., 2011). Furthermore, situations creating unwanted exposure to aerosolised nanopowders at the workplace could occur with accidental emissions representing the worst case scenarios. These cases may be unpredictable, possibly resulting in massive releases. For example the continuous, severe leakage of sub-micron particles which may occur when a tank ruptures or topples or when a pipe develops a leak. These cases of indoor accidents would dramatically increase exposure levels. So far no major indoor accidents with ENM have been reported (Nowack et al., 2014), thus the knowledge and understanding available on the dissipation behaviour of their dispersed products after an accident is limited.

With increasing interest in the accidental release of ENM to indoor environments due to potential effects on human health (Kermanizadeh et al., 2016; Oberdörster et al., 2015; Pattan and Kaul, 2014), greater attention is being paid to the development of engineering controls to protect workers. According to the National Institute of Occupational Safety (NIOSH, 2013), a hierarchy of controls should be considered and applied in order to implement effective protection of the individuals involved in the production processes of ENM. Among these, engineering controls represent the fastest response measures that protect workers from hazardous conditions. These are divided into two broad categories: ventilation and non-ventilation controls. The physical process behind ventilation, resulting in a drop in particle number concentrations after an accidental dispersion of ENM in an indoor environment is dilution. The Organization for Economical Cooperation and Development (OECD) (OECD, 2009) reviewed a

number of specific nanomaterial guidelines for laboratories and claimed that the installation of a non-recirculating ventilation system with 6 to 12 air changes per hour (ACH) combined with a negative laboratory pressurisation, are proposed where nanomaterials are handled.

Considering the ventilation process, Seipenbusch et al. (2014) calculated the evolution of the concentration of dispersed airborne particles in a fully mixed room at different numbers of ACH. For the highest ACH (20 h^{-1}), a reduction to half of the initial concentration was achieved after about two minutes. However, in a real workplace, it might be assumed that the mixing of air would not be as efficient as in the fully mixed model. Furthermore, processes such as resuspension due to air jets established by ventilation, may result in a decrease of the particle removal effect.

The level of occupant protection from accidental dispersions of ENM can be effectively controlled by the ventilation-driven airflow patterns in a workroom. According to Whicker et al. (2002), the airflow patterns have a regulatory role in the airborne concentrations of a released aerosol and in the subsequent exhaust of that from the indoor environment. Further, the level of occupant protection is enhanced by measurement techniques and strategies for the detection of unusual levels of airborne ENM in the room air. These measurement techniques and strategies have to be optimally combined to allow the sensitive determination of airborne ENM dispersed within an indoor environment. In order to achieve an effective occupant protection through the arrangement of air-samplers and real time monitors for the measurement of air quality, the knowledge of prevailing airflow patterns in the room is required (Whicker et al., 2002).

According to Ding et al. (2017), in publications between 2004 and 2016, a discussion of types of engineering controls on ENM was mostly provided as contextual information. A few of these studies also indicated a well-established framework which has informed the design aspects of the current experimental study. Bouilly et al. (2005) studied the impact of ventilation strategies on indoor particle concentrations in a cubic experimental chamber (15 m^3). They confirmed through numerical simulation that particle removal rates depended on the airflow pattern within the room. They determined that the influence of inlet and outlet location over fine particles (< 5 μm in diameter) was stronger than that for coarse particles. Zhong et al. (2010) used numerical simulation to predict aerosol dispersion in an indoor room and validated their model

against experimental data from published literature. This work examined the particle removal efficiency of two different ventilation strategies: mixing ventilation (MV) and an underfloor air distribution (UFAD) system. The air supply volume was constant (3.2 ACH) for both ventilation scenarios. The results showed that in the MV room, the indoor particles were found to be more uniformly distributed than in the UFAD room. Additionally, it was found that in both ventilation strategies the location of the source did not have a strong effect on the particle distribution, whereas airborne particles due to resuspension were detected in the MV system.

In conclusion, the existing literature indicates a strong relationship between the location of the inlet/outlet air diffusers and the established flow pattern in the indoor environment. Therefore, it could be suggested that the exposure of an individual in a room contaminated by accidentally released ENM particles would be determined by their location relative to the location of the air inlet and outlet. Furthermore, the resuspension of deposited particles due to the air jets induced by ventilation should be considered as a factor which could potentially lower the ventilation efficiency. However, there is little published understanding of optimal ventilation settings and arrangements which could ensure the most efficient particle removal in an indoor environment contaminated with dispersions of ENM. The application of ventilation strategies in a well-controlled indoor environment can support the development of indoor exposure control protocols. Such estimations can also be used in risk analysis, once ventilation efficiency and particle decay rates under various ventilation settings and measurement locations become available.

This work aims to compare different ventilation rates and their effects on airborne particle number concentrations (PNCs) and particle size distributions (PSDs) following a sustained release of aerosol originating from TiO_2 nanopowder through a heated line coupled to a nebuliser system within a 32 m^3 airtight chamber. Particular objectives are to investigate the influence of ventilation strategies and particle processes (e.g. deposition, resuspension) for particle removal within different size ranges, as well as any spatial influences (e.g. cross contamination events within the bulk region of the chamber) on particle removal mechanisms. To this end, liquid containing a pre-determined amount of suspended and processed TiO_2 nanopowder was aerosolised and injected into a mechanically ventilated indoor environment through an electrically heated delivery line from a nebuliser arrangement. The temporal variation of PNC and

PSD was tracked using three condensation particle counters (CPCs) located around the chamber and a single differential mobility spectrometer (DMS) respectively. The measurement period was divided into two stages: the aerosol injection stage and the following decay stage under different ventilation rates. The measured PSDs were de-convoluted into modes through a $\log_{10}$-normal fitting process in order to illustrate the time evolution of specific modal parameters and to extract conclusions related to the size-selectivity of the tested ventilation settings on the evacuation of the released aerosol from the indoor environment. Based on the measurements provided by the aforementioned devices, the detailed size-resolved and spatial-resolved particle decay rates, as well as the spatial ventilation efficiency, were evaluated as a function of the calibrated air exchange rate.

2. Materials and methods

2.1 Description of experimental set-up

The release of hazardous nano-particulate matter originating from specific nanopowder in accidental situations was simulated in a specially designed airtight chamber. The main test chamber (32 m^3) (Fig. 1) is constructed from prefabricated, plastic coated, wipe clean panels. This is hermetically sealed with its own inlet supply and always operates under negative pressure conditions. As shown in Fig.1a, air was supplied to the chamber through a high level wall mounted diffuser (inlet), and was extracted at a low level, diagonally opposite, through a grille of the same design (outlet). Air entering the test chamber is taken from outside the building through a pipe network and is HEPA filtered before being conditioned by a humidifier and heater, establishing a well-controlled environment to correctly interpret the acquired experimental data. The same set-up is installed for the exhaust air before being vented to the outside of the building.

The facility has six access ports situated around the walls which were used for sampling and for the introduction of nanoparticles into the chamber. When not in use, these access ports were sealed using threaded screw caps. Finally, shut-off dampers were present in both the inlet and outlet in order to ensure the internal volume was isolated during the release tests and were opened immediately before the ventilation was activated. Further details regarding the dispersion chamber are provided elsewhere (Kylafis, 2016).

Three CPCs (model 3775 by TSI Inc, USA) and a DMS (DMS500 by Cambustion ltd, UK) located at specific access ports outside the walls of the dispersion facility, were employed for the monitoring of the PNC and PSD respectively at the sampling points indicated in Fig. 1 (positions A, B and C). The CPC uses a light scattering technique to measure particles within the diameter range 4 – 3000 nm, whereas the DMS allowed measurement of PSD within the diameter range 5-1000 nm based on the particle mobility within an electric field. The aspiration rate of the DMS was 8 L/min and that of the CPC was 1.5 L/min. TSI conductive silicone tubing with 0.48 cm internal diameter (ID) was used for sampling purposes. This type of tubing effectively reduces electrostatic losses, thus diffusion loss was considered as the only major mechanism for nanoparticles during transportation. Two transport lines, each around one metre length, at positions A and B were installed at a height within the breathing zone (1.5 m above the floor), and a third one of the same length was installed at the middle of the outlet diffuser (0.55 m above the floor). Since two measurement devices (CPC and DMS) were sampling in parallel at position A, the aerosol stream was split into two via a Y connector fitted through the wall of the chamber.

The diffusion loss for particles larger than 20 nm within the transportation tubing computed by the particle loss calculator software tool (Von der Weiden et al., 2009) was less than 2 % for 1 m tubing and 1.5 L/min flow rate (position B), and less than 3.5 % for the combined flow rate (9.5 L/min) of the aerosol stream starting from position A, where the DMS and CPC were sampling in parallel. Therefore we did not implement additional corrections related to the transportation tubing. Additionally, the effect of siloxane degassing from the transportation tubing may have altered the gas composition of the sample aerosol with subsequent effects on the charging efficiency of the unipolar diffusion charger utilised by the DMS, as indicated in the work of Asbach et al. (2016). However, due to the high flow rate of aerosol sampled from position A, the concentration of emitted gas can be considered as low, reducing any potential effect on aerosol particles, as well as on subsequent sampling.

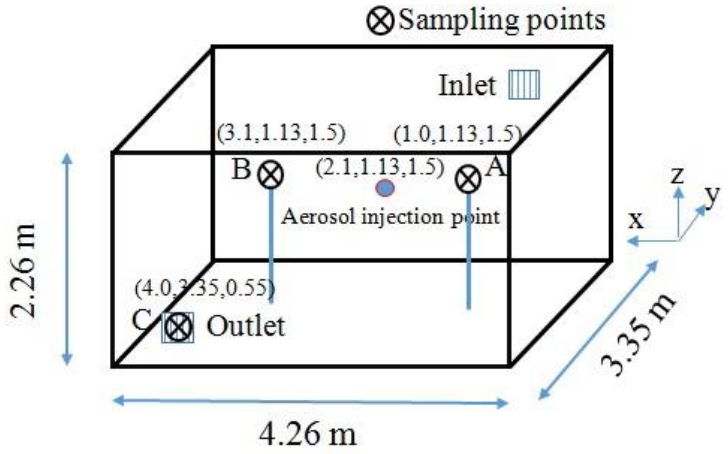

(a)

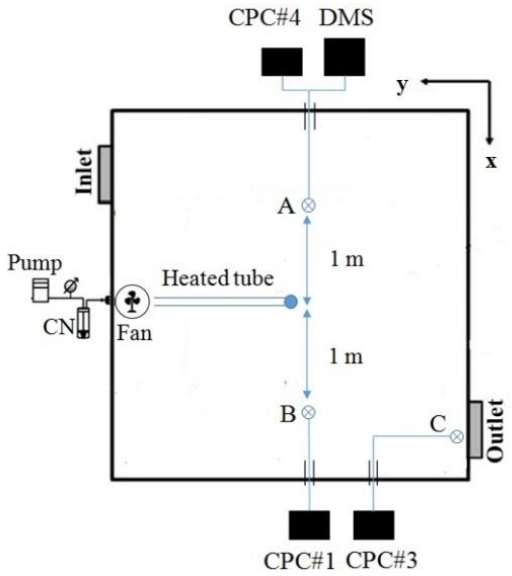

(b)

Fig. 1: (a) elevation plan of dispersion chamber indicating the coordinates of source and sampling locations and (b) floor-plan of experiment.

Inter-comparison tests between the CPCs demonstrated very good linearity and correlation between the concentrations measured by the instruments (slope 0.9-1.1 and R^2>0.97). However, inter-comparison tests between the CPCs and the DMS indicated that the latter reads higher total particle numbers compared to the former (slope 2.80 and R^2>0.99). This difference was probably most likely due to a larger fraction of nucleation mode particles (< 25 nm) resolved by the DMS compared to the CPC, and also possible differences in calibration. Price et al. (2006), who conducted comparisons of a DMS500 and CPC (model 3022A by TSI Inc., USA) also found a higher PNC reported in the response of the DMS (linearity described by a slope 1.4). These differences mean that it was not possible to provide comparative decay rates for total

PNC based on the DMS vs. CPCs. However, the DMS provides an extremely useful way of studying the time evolution of size distributions which informs understanding of the physical processes affecting the particles within the chamber.

A 6-jet Collison Nebuliser (CN, BGI Inc., USA) was attached to the inlet port used for the aerosol injection where a 1.13 m long stainless steel tube of 2.7 cm ID was fitted in order to deliver the produced aerosol at the centre of the chamber (Fig. 1). The tube was operated as a drying section by wrapping it in a heated tape at 50 ^{o}C to enhance the removal of humidity from the produced aerosol before its dispersion in the room. As will be shown below, a comparison between the particle size characteristics at the source (suspension) and of those at the airborne phase during the early stage of release, facilitated the evaluation of the drying process applied on the generated aerosols.

A Tinytag Ultra 2 TGU-4500 data logger was placed at the sampling point of the position A to record the temperature and relative humidity during the experiments. Inlet temperature was relatively constant throughout the experiments (22.66 ± 0.25 ^{o}C). The relative humidity was 56 ± 4 % RH and 61 ± 6 % RH, throughout the injection and ventilation period, respectively. The nebuliser utilised a separate pump, pressure regulator and meter operating at a flow rate of 8 litres min^{-1} to deliver HEPA filtered air for the carrier gas. A household fan at the bottom of the chamber was operating during the experimental process in order to establish good mixing conditions of the injected aerosol. According to the measurement obtained by a hand held anemometer (Kestrel 1000 by Kestrelmeter, USA), the induced velocity of air by the fan was 4 ms^{-1}.

Considering that the calibrated ventilation rate of the particular chamber varied from 0.5 to 12 ACH and the need for low background (BG) particle concentrations, the chamber was ventilated for a 10 min period at the highest ACH rate prior to each experiment. In this way, it was ensured that any elevated PNC in the chamber was due to the aerosol release process. The CPC devices were used to sample air from the room prior to the release process. The spatial indoor BG PNC reached a stable concentration of less than 1000 particles/cm^3 at 12 ACH.

The devices were scheduled to start the monitoring process at a specific time and the 6-jet CN was then filled with 50 ml of the sonicated TiO_2 nano-suspension whose production method is described below. The indoor environment was isolated through

the shut-off dampers and TiO_2 nano-aerosol was injected continuously for 70 min. This particular length of the injection process was deduced from the required duration for filling the chamber with aerosol concentration enough to accurately measure the concentration decay in the chamber, but not so high that coagulation would be appreciable. When the injection process was complete, the dampers were immediately turned on and the ventilation system was activated. For each ventilation setting, instruments sampled until the PNC dropped to a plateau level and the dispersion chamber was deemed to have reached its steady-state where no further extraction of particulates could be achieved by the ventilation system. Three replicate runs for each ventilation rate were conducted.

2.2 Generation of airborne sub-micron particles

Samples of Aeroxide TiO_2 P25 nanopowder (average primary particle size 21 nm and specific surface area 50 ± 15 m^2/g) were obtained. A method standardised by the National Institute of Standards and Technology (NIST) (Taurozzi et al., 2012) for the preparation of nanoparticle dispersions of TiO_2 nanopowders was utilised with some small modifications due to the different characteristics of the equipment used in this work. As the particular method has been validated for the preparation of aqueous dispersions in the (0.5-20) mg/mL concentration range, dispersions of the highest powder concentration (20 mg/mL) were prepared by suspending a weighed amount of TiO_2 nanopowder (1 g) in 50 mL of Type I biological grade de-ionised water (≥18 MΩcm resistivity) within a 50 mL cylindrical glass beaker. The beaker was placed in a bath with crushed ice and water, and fixed in the centre of the bath using clamps.

Initially, the 20 mg/mL suspension was sonicated for 15 minutes, as proposed by the protocol, via an ultra-sonic processor UP 100H (Dr. Hielscher GmbH, Germany) which yields a delivered power of approximately 100 W. However, particle size characterisation conducted through the method discussed below, indicated the presence of a small fraction of particles within the μm-range. Therefore, the length of sonication was increased (from 15 to 30 minutes) and new measurements indicated the elimination of coarse particles. We concluded that the extension of the sonication length was required due to the fact that the sonotrode of the particular device used in this work had a tip diameter of 7 mm, half of that (14 mm) utilised in the NIST preparation method. Longer times than 30 minutes were not considered as the goal of this work was the

elimination of larger particles, and the enhancement of fractions of sub-micron particles in the suspensions.

In order to evaluate the effect of the sonication process on the de-agglomeration of powder in the liquid and the electrostatic stabilisation of the produced liquid dispersions before their nebulisation, dynamic light scattering (DLS) and pH measurements were performed respectively. Sonicated samples were prepared in triplicate, while three unsonicated samples were utilised as reference suspensions. A Zetasizer Nano ZS (Malvern Instruments Ltd., Worcestershire, UK) was utilised for the measurement of the volume-based PSDs. Finally, comparisons between the average volume-based PSDs in the sonicated suspensions, obtained from the Zetasizer, and the averaged number-based PSDs measured by the DMS in the airborne phase over the first 10 minute intervals of the total number of the release tests, facilitated the evaluation of efficiency of the drying process applied on the generated aerosols.

2.3 Modal parameter fitting procedure

In order to study the evolution of the component modes during the ventilation period, as well as the temporal characteristics of the accumulated aerosol over a short period before the start of ventilation, modal fits were obtained for the PSDs measured by the DMS. PSDs from monodisperse sources have been shown to be mathematically described by $\log_{10}$-normal distributions. Since the present work studies airborne nanomaterial particles originating from nanopowders, following airborne processing, their diameters were expected to range over several orders of magnitude. Therefore, as indicated by other outdoor atmospheric studies (Agus et al., 2007; Lingard et al., 2006; Whitby, 1978), this wide range of particle diameters results in a better description of the PSD using a sum of $\log_{10}$-normal size distributions. This approach allows the PSD to be described by a small number of parameters. A modal fitting program, Rmixdist, was used within this study to estimate the modal PNC (mPNC), count median diameter (CMD) and geometric standard deviation (σ_g) of the modes within the measured PSDs. The full attributes of the program are described in Leys et al. (2005).

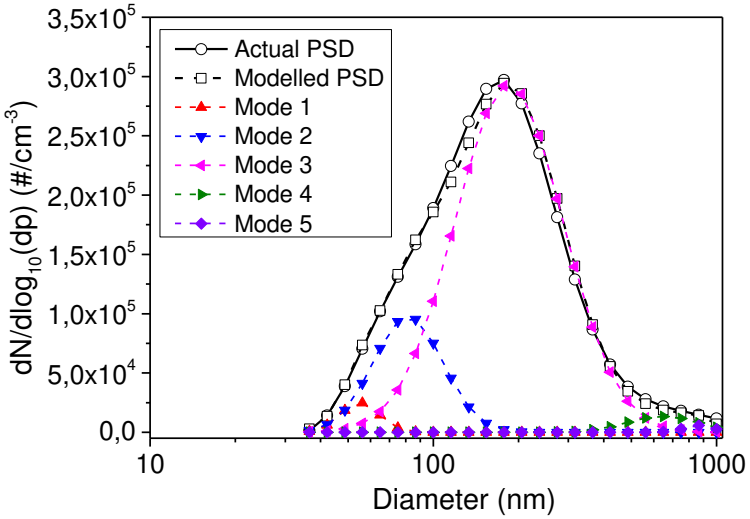

Fig. 2: An averaged PSD over a 10 minute interval of a typical TiO_2 dispersion test, indicating the component log_{10}-normal modes fitted by the Rmixdist package.

The number of fitted modes required to accurately model the measured PSD varied between four and six. An example of a campaign averaged PSD over a 10 minute interval during the injection of TiO_2 aerosol into the dispersion chamber, along with the log_{10}-normal component modes fitted by Rmixdist, is shown in Fig. 2.

2.4 Estimation of the particle decay rate

The decay of an instantaneously released aerosol into a well-mixed and air-tight enclosure can be described as:

$$C(t) = C_0 \exp(-\beta t) \qquad (1)$$

where β is the total particle decay rate (h^{-1}), t is the elapsed time and C_0 is the initial indoor particle concentration (particles/cm^3) at time t=0 (end of injection).

Given that deposition is more efficient and faster than coagulation in removing particles (Nikolova et al., 2014), in this work, for the measurements obtained by the DMS, we considered that for each determined size group, β represents the ventilation and deposition sink, with the ventilation being the dominant one, as well as some secondary contributions of mechanisms, such as resuspension, which may result in particle gain and subsequently in the decrease of the total particle decay rate. The accuracy of the fit through the use of Eq. (1) on the size-resolved data obtained from the DMS was described by the high values of R^2 (>0.97).

However, in respect of the data obtained from the distributed CPCs, a low fitting accuracy was observed. This could be attributed to the fact that a CPC provides size

integrated PNC within the diameter range 4 – 3000 nm. Therefore different particle decay rates originating from the contributions in the different sizes of the total PNC decay could be considered. In the absence of a model that may lead to meaningful physical information, we fitted the CPC data using bi-exponential functions incorporating a weighing factor to account for the relative contribution of each term in the total PNC decay. These functions are described by the following general form:

$$C(t) = C_0[(X\exp(-\beta_1 t) + (1-X)\exp(-\beta_2 t)] \qquad (2)$$

where X is the weighting factor with values that fall between zero and one, β_1 is the primary decay rate representing the fast removal mechanisms such as ventilation and deposition, whereas β_2 is a secondary decay rate, substantially lower than β_1 in terms of absolute values.

Since the distributed CPCs provided PNC measurements with spatial resolution, and due to the potential mass exchange of particulate matter (cross contamination events) between the different sampling regions centred at positions A and B (Fig. 1), we considered that β_2 includes mechanisms leading to both particle loss (e.g. losses due to cross contamination episodic events), or particle gain (e.g. resuspension or particle gain due to introductions induced by the cross contamination episodic events). It is understood that the former implies positive values for β_2, whereas the latter implies negative values for β_2. A typical plot of fitting for PNC vs. time for a test at 3 ACH using mono- and bi-exponential decay is shown in Fig. 3. As can be seen, a significantly higher fitting accuracy (R^2=0.99) occurred through the use of a bi-exponential function compared to that (R^2=0.91) which occurred through the mono-exponential one.

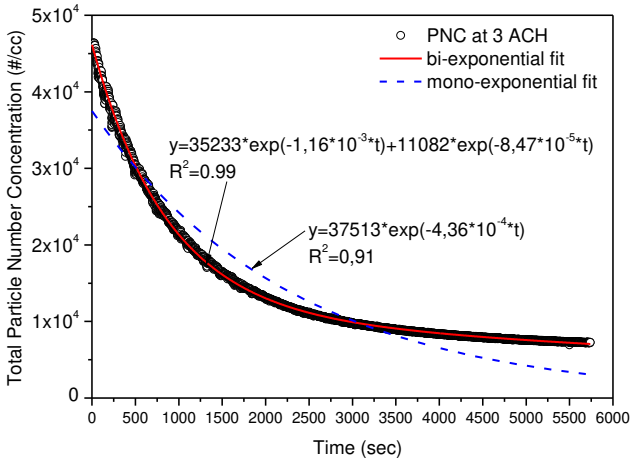

Fig. 3: Mono- and bi-exponential fittings to the PNC decay curve corresponding to 3 ACH test. Fitting parameters are shown in the figure

2.5 Estimation of the ventilation efficiency

The concept of ventilation efficiency provides a useful tool for the evaluation of the performance of ventilation systems in an indoor environment. Chung and Hsu (2001) referred to this parameter as an indicator of the mixing characteristics of incoming air with air already present inside an indoor environment. Ventilation efficiency may also be used for the characterisation of the indoor contaminant distribution resulting from the interaction of the supplied air with internal pollutant sources. In this work, the definition of ventilation efficiency introduced by Sandberg (1981) was used. Using values from steady-state conditions, the relative ventilation efficiency at a given point in an indoor exposure zone may be defined as:

$$E = \frac{C_e - C_s}{C_i - C_s} \qquad (3)$$

where E is the relative ventilation efficiency at the sampling points, C_e is the contaminant concentration in the exhaust diffuser, #/cm^3; C_s is the contaminant concentration in the supply diffuser, #/cm^3, and C_i is the contaminant concentration at the indoor sampling points, #/cm^3. In this study, C_i was represented by the PNC measurements obtained by CPC#4 (position A) and CPC#1 (position B), while C_e was represented by CPC#3 (position C) which was sampling at the outlet diffuser during the tests. Regarding the C_s quantity, separate 10-minute tests under the studied ventilation rates were conducted, by installing the sampling line of CPC#4 on the supply diffuser. These measurements were averaged over the specified periods for each ventilation rate and introduced as constant inputs into Eq. 3 for the estimation of the ventilation efficiency at the positions A and B.

3. Results and discussion

3.1 Material characterisation

The averaged volume-based distributions as measured by the DLS technique over the three sonicated and three unsonicated TiO_2 samples (suspension phase), as well as the averaged number-based distribution over the first 10 minute periods of the total number of the injection tests (airborne phase), are presented in the double-y axis graph in Fig. 4. It should be noted that for the DLS technique, if the number distribution consists of

two peaks of a 1:1 ratio, then in the respective volume distribution, the two peaks change to 1:1000 ratio as the volume of a sphere is proportional to the third power of the particle diameter (hydrodynamic diameter). On the other hand, the DMS technique determines number concentration distributions of airborne particles as a function of electrical mobility diameter, after nebulising the suspension into air.

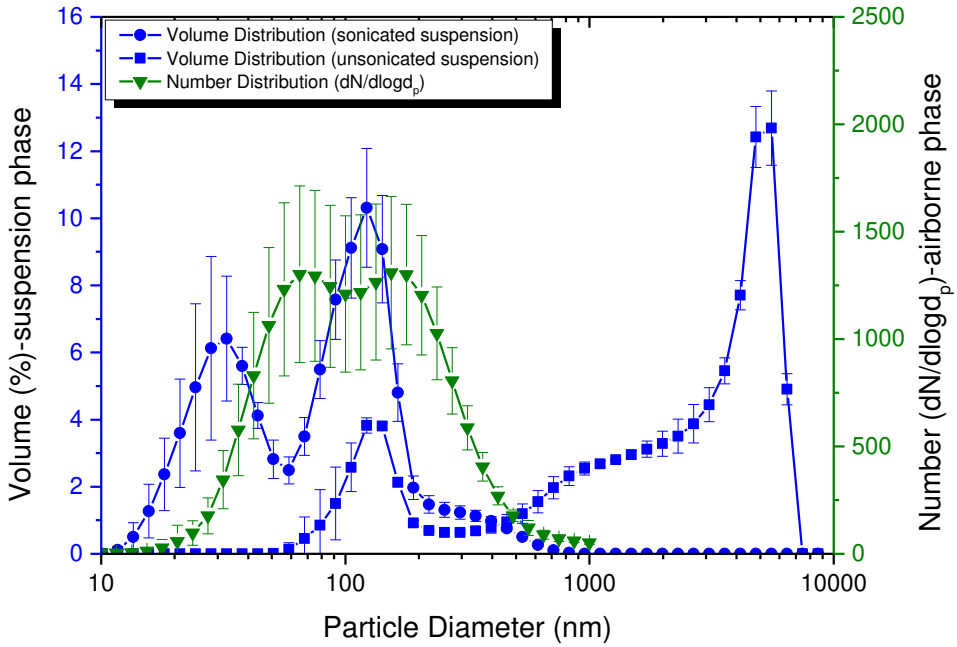

Fig. 4: Volume and Number based average PSDs derived by the DLS method (sonicated and unsonicated suspension phase) and the DMS method (airborne phase), respectively (symbols: experimental data ±2σ; line: multiple peak fit).

As can be seen in Fig.4, the un-sonicated sample exhibited a broad polydisperse and multimodal PSD, predominantly described by the presence of particles in the (1-10) μm range. The sample typically had a major fraction of agglomerates centred at around 5220 nm and a minor fraction of particles with a peak centred around 132 nm. Fragmentation occurred in suspension after undergoing sonication resulting in a multimodal distribution and in the presence of particles < 100 nm. The sonicated suspension presented a secondary peak centred at 33 nm (quite close to the 21 nm primary particle diameter in the powder form as specified by the manufacturer) of a volume fraction (6.5 %), while the main peak (122 nm) exhibited a volume approximately equal to 10.3 %. Additionally, the elimination of the microscale component fraction, achieved through the sonication process, can be observed. Also, according to NIST (Taurozzi et al., 2012), the final pH of the P25 aqueous dispersion

should be between 3.7 and 4.9 in order to obtain a suspension that is electrostatically stabilised. Measurements conducted on the sonicated samples prepared in this work indicated that pH was in the range of 4 ± 0.25.

According to the above, the ultra-sonication of an agglomerated cohesive nanopowder in water was shown to be sufficient to de-agglomerate the stored nanoparticles and to enable the production of nano-suspensions characterised by large fractions of particles with diameter ≤ 100 nm. At the same time, this method resulted in the elimination of the presence of particles in the micron scale and in the establishment of electrical stability in the produced suspensions.

After nebulising the sonicated suspension into air, the generated aerosol presented two main peaks, the first centred at 65 nm and the second at 154 nm (see Fig.4). Therefore, considering the increase of diameter caused by the possible residues in suspensions (Fissan et al., 2014), it seems quite reasonable to consider that the installed heated line at the outlet of nebuliser provided sufficient evaporation of any remaining water from the droplets leading to the presence of solid particles within the generated aerosols before their introduction into the dispersion chamber.

3.2 Aerosol emission tests and aerosol characterisation

The average temporal variations of PNCs tracked by the CPCs sampling within the breathing zone on both sides (positions A and B) of the injection point, are shown in Fig. 5. These measurements describe the overall experimental period divided into two stages: the injection and the cleaning stage of the chamber through mechanical ventilation. The standard deviations are shown as whiskers indicating the variability between the different injection tests. Measurements conducted at position C are not included as the device employed there was sampling at a height not representative of an exposure scenario and as indicated above these measurements were used as inputs for the estimation of the ventilation efficiency at the positions A and B.

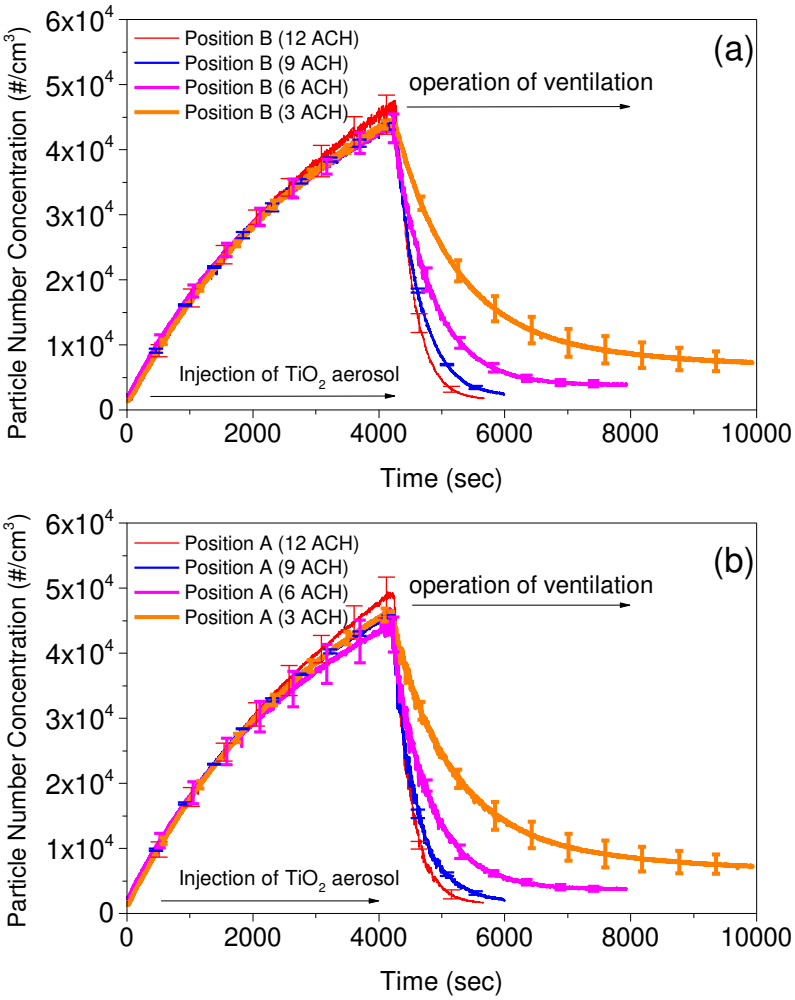

Fig. 5: Temporal variation of the average PNCs in the dispersion chamber during the overall experimental period as measured by the CPCs at a) position B and b) position A (line: experimental data ± 2σ).

According to Figs. 5a and 5b, once the aerosol particles were emitted into the dispersion facility they spread throughout the room within a few seconds causing the concentrations at both measurement positions to rise rapidly. The period after the shut-off of the nebuliser was described by an exponential decay of the PNCs. As outlined in the introduction section, dilution due to ventilation is a major process in reducing the concentration levels of dispersed ENM emissions in workplaces. Therefore, as was expected, at the highest ventilation rate (12 ACH) the induced dilution resulted in the fastest decay of the PNCs in the chamber.

However, it is interesting to notice the leftover particles suspended in the air at the end of the ventilation process varying with the number of the ACH. For the highest ventilation rates (12 ACH and 9 ACH), the chamber was evacuated down to levels of

PNC close to the initial background particle concentrations before the start of injection. However, for the lower ventilation rates (6 and 3 ACH), at the end of the decay process, measured PNCs were relatively higher than the background PNC (measured before the release) at both sampling locations (increased by a factor of approximately one and five, at 6 and 3 ACH, respectively).

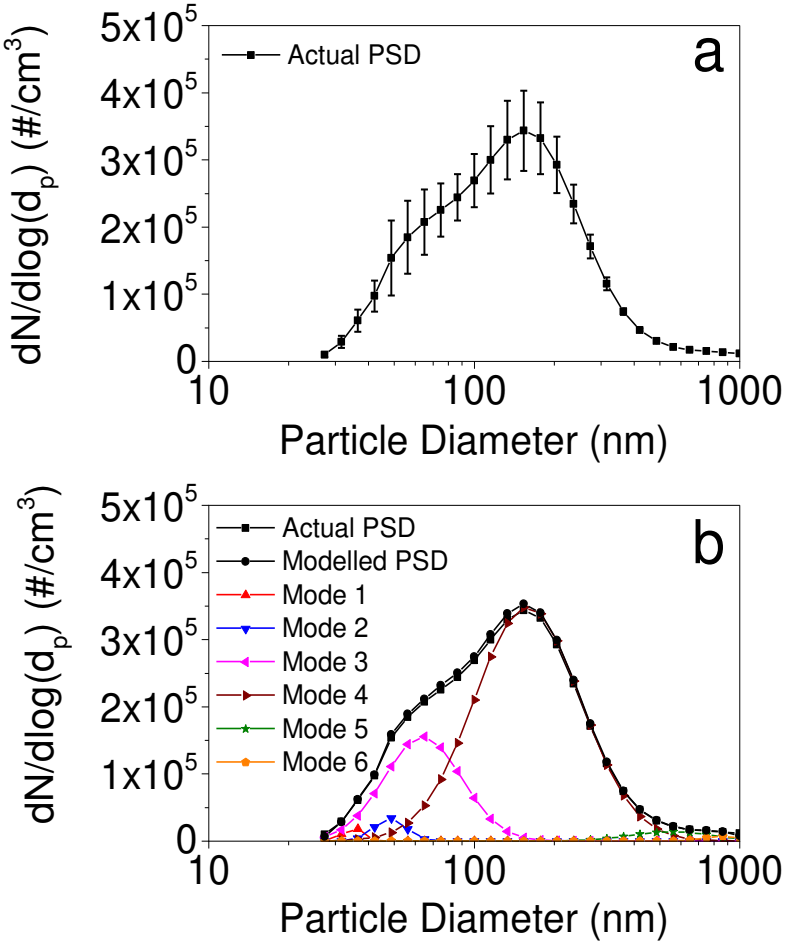

Fig. 6: a) Actual PSD obtained by the DMS, averaged over the last 10 minute period of injection and b) modelled PSD along with the modes present within the actual PSD as estimated by the Rmixdist program (open dots: experimental data ± 2σ; line: lognormal fitting).

The averaged number based PSD measurements over the last 10 minute period of injection obtained by the DMS (position A) are presented in Fig. 6a. Fig. 6b shows the modal groups present within the measured/actual average PSD (Fig. 6a), using $\log_{10}$-normal distributions as estimated by the Rmixdist program. Results suggest that the PSD can be de-convoluted into 6 modes with *CMD*s of 34 nm, 48 nm, 64 nm, 158 nm,

555 nm and 860 nm, while the average percentage contribution of each mode to total PNC was 0.74%, 2.07%, 23.2%, 71.5%, 2.05% and 0.46%, respectively.

Using the modal fits, the evolution of the mPNC grouped into fine (diameter > 100 nm) and ultrafine (diameter ≤ 100 nm) particles during the decay period under evacuation by the specified ventilation rates, can be seen in Fig. 7. This allows the evaluation of the selective removal behaviour of the tested ventilation rates on the specified particle size groups, especially on ultrafine particles which once inhaled due to their small size are able to pass into the deeper region of the human respiratory tract resulting in the higher probability of adverse health effects because of particle-tissue and particle-cell interactions (Blank et al., 2009).

As shown in Fig. 7, at the highest ventilation rate (12 ACH) the evacuation of ultrafine particles was more effective than for fine ones. 12 and 20 minutes were required for the mPNC of ultrafine and fine particles respectively, to be decreased to almost zero by the ventilation system. On reducing the ventilation rate from 12 to 9 ACH, a significant increase in the evacuation time was demonstrated for both size groups. 35 minutes were required for mPNC of both size groups to be decreased to almost zero by the ventilation system. Therefore, results here suggest that the induced removal efficiency of ventilation for the ultrafine particles was more sensitive to the decrease of ventilation power compared with that for the fine ones.

On further decreasing the air exchange rate, the removal efficiency of the ventilation system was further decreased, especially for the ultrafine particles. Indicative of this trend is that at 3 ACH (see Fig. 7b) 30 min after the activation of the ventilation system, the mPNC of ultrafine particles had dropped to only 60 % of the initial peak concentration. At the same time, fine particles had reached 30 % of their initial peak concentration. As a result, fractions of these particles remained suspended in the air maintaining exposure at relatively high levels even after a complete evacuation. This trend could be attributed to the strong diffusion characteristics demonstrated by ultrafine particles (Hinds, 1982) and their subsequent capability to escape from a low strength ventilation flow field, such as established at 3 ACH.

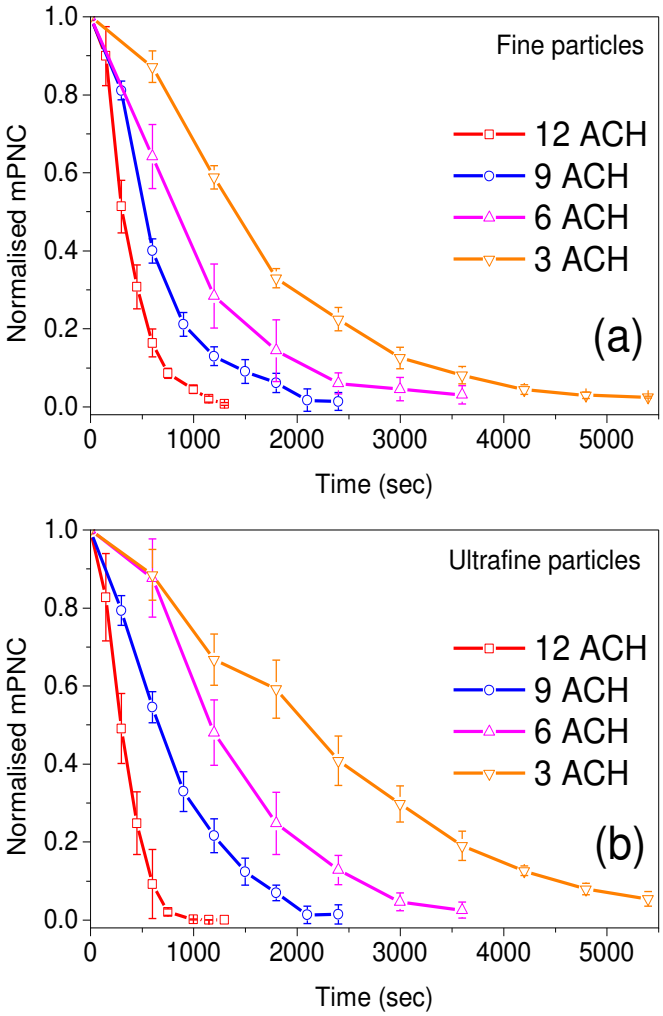

Fig. 7: Evolution with time of the normalised mPNC under different ventilation rates for, a) fine, and, b) ultrafine TiO_2 aerosol particles (open dots: experimental data ± 2σ).

3.3 Particle decay rates

The average particle decay rates (β) estimated for each size channel of the DMS, were averaged over more extended size bins as presented in Fig. 8. Considering that the test chamber has been calibrated for the studied air change rates and that the air introduced into the chamber is almost particle free, it is expected that the measured decay rates would be equal or greater to the number of ACH.

As shown in Fig. 8a, for 12 ACH, all size bins presented decay rates higher than the air exchange rate indicating the action of strong deposition, especially for the smallest size bin 5-100 nm (ultrafine particles) whose decay rate was significantly higher (16.4 h^{-1}) than the ventilation particle sink (12 h^{-1}). The strong air flow fields in the chamber induced by the combined operation of the mechanical ventilation and the fan, enhanced

the losses of smaller particles where deposition is dominated by diffusion (Hinds, 1982) resulting in decay rates higher than the established ventilation sinks. Similar observations were made in the study conducted by Gong et al. (2009) in vehicles. Specifically, the authors indicated that the deposition rates of ultrafine particles increased when the in-cabin air velocity was increased, with the highest increases occurring for smaller particles due to their greater diffusional deposition.

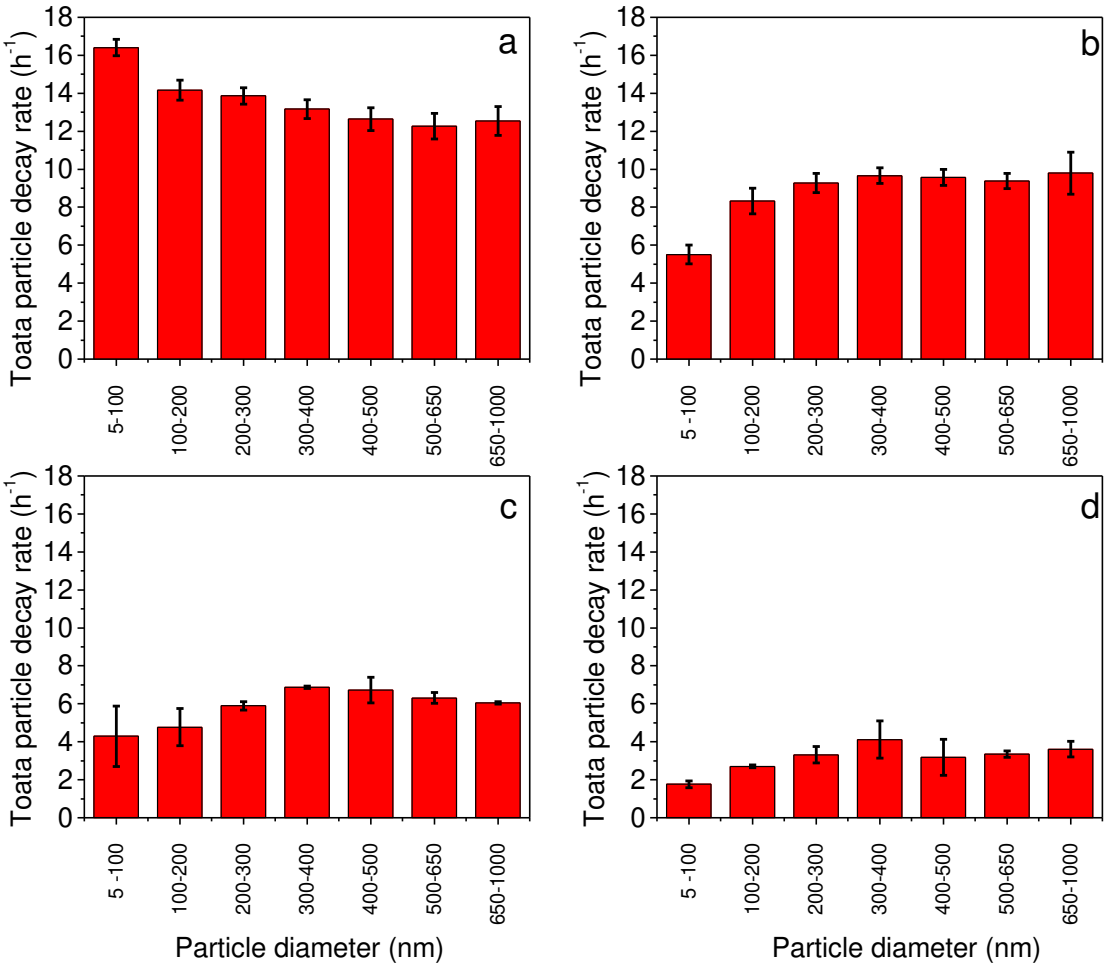

Fig. 8: Average particle decay rates β (h^{-1}) estimated from the measurements obtained by the DMS for ventilation rates a) 12 ACH, b) 9 ACH, c) 6 ACH, and, d) 3 ACH (error bars: experimental data ± 2σ).

When the ventilation rate was decreased from 12 to 9 ACH, the majority of size bins demonstrated decay rates relatively higher than the corresponding ventilation sink (9 h^{-1}) apart from the two lowest size bins (see Fig. 8b). Considerably strong air flow velocities induced by the specified number of air changes combined with the fan operation throughout the experimental period, may have resulted in the resuspension of particles into the bulk region of the chamber. Resuspension of particles could also be

considered at 12 ACH; however, the fast evacuation rate induced at such a high ventilation power may result in the fast removal of these particles and consequently their lack of detection by the DMS.

By decreasing the ventilation rate from 9 to 6 ACH, more bins from the lowest size region were introduced into the group of those which demonstrated decay rates lower than the corresponding ventilation sink (see Fig. 8c), indicating a critical point where the influence of the combined action of mechanical ventilation and fan operation on the resuspension of particles had a maximum effect due to the weakness of the ventilation system to efficiently remove the resuspended particles from the indoor atmosphere. Also, it is interesting to note that in the group of affected bins was the one that contained the mode of the highest particle population (100-200 nm). Finally, at the lowest ventilation rate (3 ACH), when the power of mechanical ventilation was further reduced and consequently the level of the induced turbulence, it is possible that resuspension of particles was mainly induced by the fan, dropping the number of the affected bins from three to two (see Fig. 8d).

Based on the above it is suggested that the smaller particles were more efficiently removed when the air exchange rate was at the maximum (12 ACH) due to the combination of ventilation with their increased turbulent deposition at such a high ventilation rate. As an example for nanoscale particles, those in the size bin 5-100 nm had removal efficiencies of >100%, 61.1%, 71.6% and 58.6%, at 12, 9, 6 and 3 ACH, respectively, compared to those in the size bin 650-1000 nm, which demonstrated removal efficiencies >100% independent of the number of ACH.

Due to increased turbulent deposition, surface contamination should be carefully considered as deposited particles could provide a secondary emission source in post-accidental conditions (Shepard and Brenner, 2014). Furthermore, special attention should be given in the case of the application of moderate ventilation rates, such as 6 ACH. The turbulence induced by the mechanical ventilation along with other sources of turbulence which are likely to occur in a real workplace (turbulence generated by the industrial process itself), may result in the resuspension of smaller particles and subsequently in an increase in their airborne lifetime.

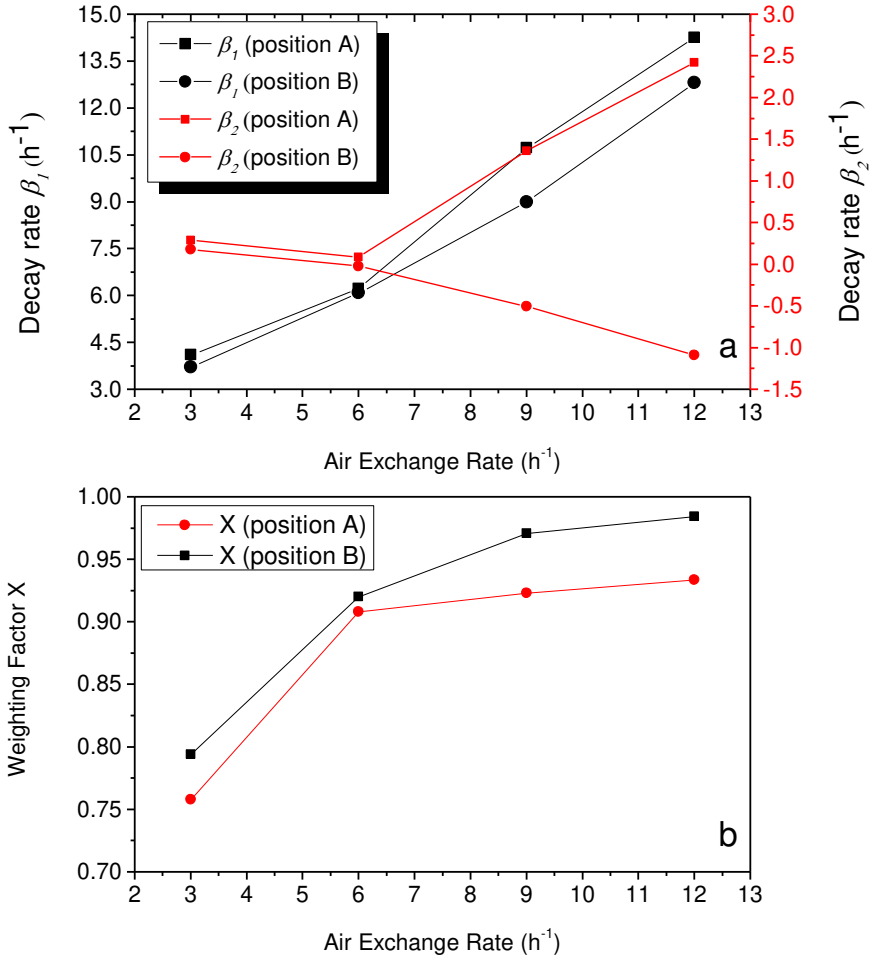

Fig. 9: The change at positions A and B of a) particle decay rates (β_1 and β_2) and, b) the weighing factor X, with the air exchange rate.

Although not size-resolved, the particle decay rates and the weighting factor X with the air exchange rate as derived from the bi-exponential fits to the data obtained from the distributed CPCs (positions A and B), are given in Fig. 9. According to Fig. 9a, at the highest ventilation rates (12 and 9 ACH), the particle decay rate β_1 at position A (14.25 and 10.72 h^{-1} at 12 and 9 ACH respectively) was substantially higher than that at position B (12.81 and 9.10 h^{-1} at 12 and 9 ACH respectively). This is an indication of the stronger particle deposition occurred in the area of the former compared to that in the area of the latter.

Based on the work conducted by King et al. (2013), experimental measurements in the chamber used in this work, indicated that the air velocity profile in the region of position A was generally higher than that in the region of position B, due to the impinging jet from the inlet diffuser. Therefore, as also indicated in the size-resolved particle decay rates, it is reasonable to consider that increased turbulent deposition of the smaller

nanomaterial particles occurred at position A compared to that at position B, due to the increased air velocity in the former compared to that in the latter at high ACH.

At the same time, in respect of the particle decay rates β_2, a completely different trend between the two positions can be seen. Specifically, the particle decay rate β_2 at position A demonstrated positive values (2.42 h^{-1} and 1.36 h^{-1}, at 12 and 9 ACH respectively), while at position B demonstrated negative values (-1.1 h^{-1} and -0.5 h^{-1}, at 12 and 9 ACH respectively). Therefore, we conclude that at such high ventilation rates, due to the establishment of rapid mixing conditions close to the inlet diffuser, cross-contamination induced by the dispersion of small fractions of aerosol particles to regions where mixing conditions are poor, should be considered. These regions could operate as particle traps where localised poor ventilation might occur at high air exchange rates. At the lowest ventilation rates (6 and 3 ACH), a convergence between the values of particle decay rates β_1 and β_2 corresponding to positions A and B, can be seen (Fig.9a), indicating a balance in the spatial characteristics of PNC decay in the chamber independent of the sampling location.

Finally, regarding the weighting factor *X*, as shown in Fig. 9b, at the highest air exchange rates (12, 9 and 6 ACH) the dominant role of ventilation in the particle removal is confirmed by the high values of the particular parameter at both sampling positions (over 90% contribution in the total particle sink). However, at the lowest air exchange rate (3 ACH), the ventilation strength plunged below 80% at both sampling positions (75.8% and 79.4% at position A and B respectively), and this is subsequently associated with the maintenance of relatively high PNC at the end of the evacuation period, as indicated by the CPCs measurements.

3.4 Spatial ventilation efficiency

The spatial variation of the average ventilation efficiencies corresponding to the different ventilation rates are presented in Fig. 10. The results indicate that at high ventilation rates, the position A close to the inlet diffuser exhibited the highest ventilation efficiency compared to that at position B. However, by decreasing the ventilation power, the relative difference between the ventilation efficiency of the two sampling points was observed to gradually decrease. Finally, at 3 ACH the two values became almost equal indicating that ventilation efficiency at such a low ventilation rate

is independent of sampling location. It is clear that the sampling point close to the air inlet demonstrated higher sensitivity to the decrease of the ventilation power compared to that located far from the inlet diffuser. This seems to be caused by the fact that at position A concentration variation closely followed the inlet ventilation level (dilution rate), while at position B the dilution rate allowed more time for particles to mix in the chamber.

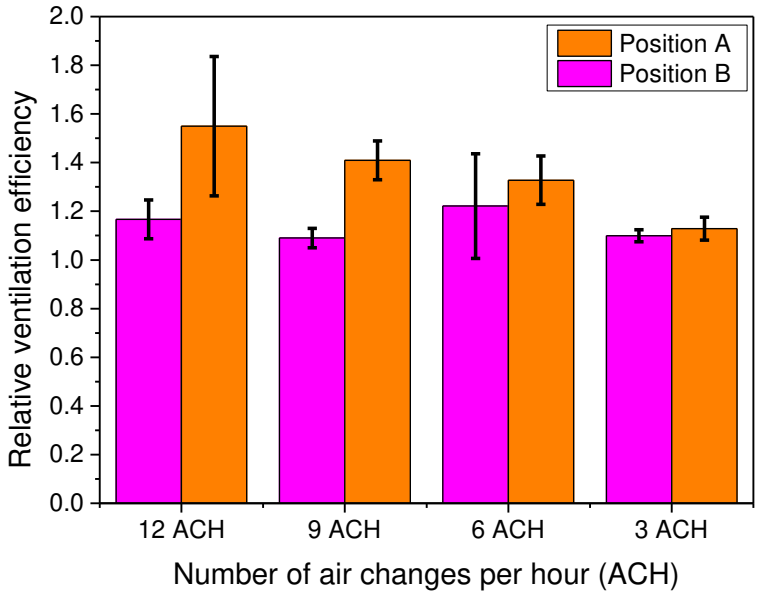

Fig. 10: The ventilation efficiency at positions A and B under the different studied ventilation conditions (error bars: experimental data ± 2σ).

4. Conclusions

The accumulation and clearance of dispersed airborne nanomaterial particles generated from processed nanopowder samples, has been shown in this study to be proportional to the overall room ACH rate, and significantly influenced by the direction and velocity of room air currents. Of the ACH rates evaluated, the greatest relative improvement in particle concentrations and clearance time occurred at the highest ventilation rate (12 ACH). However, regions close to the inlet diffuser at such a high ventilation rate would suffer from surface contamination due to the increased turbulent deposition induced by the strong mixing conditions. This further reinforces the suggestion that surfaces at a nanotechnology workplace should be carefully cleaned, even after a complete evacuation at high ventilation rates, since deposited particles could provide a secondary emission source under post-accidental conditions. Finally, indications of cross-contamination from regions with strong mixing conditions to regions where mixing was

poor were obtained, showing that the latter could operate as particle traps where localised poor ventilation might occur at a high air exchange rate. This hypothesis was confirmed by the calculation of the location specific ventilation efficiencies as a function of ACH which indicated that at high ventilation rates, optimal ventilation occurs closer to the inlet diffuser.

Reducing the ventilation rate resulted in an increase of leftover particles in the air of the chamber when the ventilation process had been completed. Interestingly it was shown that a gradual decrease in ventilation strength led to an increased ratio of ultrafine particles over fine ones and subsequently to dangerous accumulation of contaminants with high exposure hazards. Furthermore, the size-resolved particle decay rates indicated that the lower size bins were affected by this gradual decrease with the maximum number of affected bins occurring at 6 ACH. We considered this as an indication of resuspension induced by the synergistic effect between the different turbulent sources within the chamber (mechanical ventilation and household fan). This synergy demonstrated a maximum effect at a moderate ACH rate when the ventilation system was not efficient enough to quickly remove the resuspended particles, but at the same time was efficient enough to generate turbulence that along with a constant turbulent source promoted resuspension. Finally, by decreasing the ventilation rate, ventilation efficiency was shown to be gradually independent of the distance to the inlet diffuser, indicating a well mixed state of airborne particles throughout the chamber. This suggests that the re-engineering of supply and exhaust air diffusers can be an effective means to functionally increase the efficiency of the ventilation system at nanotechnology workplaces and potentially allows for designs at lower ACH rates.

Acknowledgments

The authors would like to thank the European Commission 7th Framework program for Research and Technological Development NMP under grant agreement FP7-NMP-2010-LARGE-4, № 263215.

Note: The present paper reflects only the authors' views and the Union is not liable for any use that can be made of the information contained therein.

References

Agus, E.L., Young, D.T., Lingard, J.J., Smalley, R.J., Tate, J.E., Goodman, P.S., Tomlin, A.S., 2007. Factors influencing particle number concentrations, size distributions and modal parameters at a roof-level and roadside site in Leicester, UK. Science of the total environment 386, 65-82.

Asbach, C., Kaminski, H., Lamboy, Y., Schneiderwind, U., Fierz, M., Todea, A.M., 2016. Silicone sampling tubes can cause drastic artifacts in measurements with aerosol instrumentation based on unipolar diffusion charging. Aerosol Science and Technology 50, 1375-1384.

Blank, F., Gehr, P., Rothen-Rutishauser, B., 2009. In vitro human lung cell culture models to study the toxic potential of nanoparticles. Nanotoxicity: From in vitro, in vivo models to health risks. Chichester, England: Wiley, 379-395.

Bouilly, J., Limam, K., Béghein, C., Allard, F., 2005. Effect of ventilation strategies on particle decay rates indoors: An experimental and modelling study. Atmospheric Environment 39, 4885-4892.

Chung, K.-C., Hsu, S.-P., 2001. Effect of ventilation pattern on room air and contaminant distribution. Building and Environment 36, 989-998.

Ding, Y., Kuhlbusch, T.A., Van Tongeren, M., Jiménez, A.S., Tuinman, I., Chen, R., Alvarez, I.L., Mikolajczyk, U., Nickel, C., Meyer, J., 2017. Airborne engineered nanomaterials in the workplace—a review of release and worker exposure during nanomaterial production and handling processes. Journal of hazardous materials 322, 17-28.

Fissan, H., Ristig, S., Kaminski, H., Asbach, C., Epple, M., 2014. Comparison of different characterization methods for nanoparticle dispersions before and after aerosolization. Analytical Methods 6, 7324-7334.

Gong, L., Xu, B., Zhu, Y., 2009. Ultrafine particles deposition inside passenger vehicles. Aerosol Science and Technology 43, 544-553.

Kermanizadeh, A., Gosens, I., MacCalman, L., Johnston, H., Danielsen, P.H., Jacobsen, N.R., Lenz, A.-G., Fernandes, T., Schins, R.P.F., Cassee, F.R., Wallin, H., Kreyling, W., Stoeger, T., Loft, S., Møller, P., Tran, L., Stone, V., 2016. A Multilaboratory Toxicological Assessment of a Panel of 10 Engineered Nanomaterials to Human Health—ENPRA Project—The Highlights, Limitations, and Current and Future Challenges. Journal of Toxicology and Environmental Health, Part B 19, 1-28.

King, M.-F., Noakes, C., Sleigh, P., Camargo-Valero, M., 2013. Bioaerosol deposition in single and two-bed hospital rooms: A numerical and experimental study. Building and Environment 59, 436-447.

Kuhlbusch, T.A., Asbach, C., Fissan, H., Göhler, D., Stintz, M., 2011. Nanoparticle exposure at nanotechnology workplaces: a review. Particle and Fibre Toxicology 8, 1.

Kylafis, G.F., 2016. The Explosion and Dispersion Potential of Engineered Nanoparticles, PhD thesis. University of Leeds. Available at: http://etheses.whiterose.ac.uk/15618/.

Leys, J., McTainsh, G., Koen, T., Mooney, B., Strong, C., 2005. Testing a statistical curve-fitting procedure for quantifying sediment populations within multi-modal particle-size distributions. Earth Surface Processes and Landforms 30, 579-590.

Lingard, J.J., Agus, E.L., Young, D.T., Andrews, G.E., Tomlin, A.S., 2006. Observations of urban airborne particle number concentrations during rush-hour conditions: analysis of the number based size distributions and modal parameters. Journal of Environmental Monitoring 8, 1203-1218.

Nikolova, I., Janssen, S., Vos, P., Berghmans, P., 2014. Modelling the mixing of size resolved traffic induced and background ultrafine particles from an urban street canyon to adjacent backyards. Aerosol and Air Quality Research 14, 145-155.
NIOSH, 2013. Current strategies for engineering controls in nanomaterial production and downstream handling processes. Cincinnati, OH: U.S. Department of Health and Human Services, Centers for Disease Control and Prevention, National Institute for Occupational Safety and Health, DHHS (NIOSH) Publication No. 2014–102.
Nowack, B., Mueller, N.C., Krug, H.F., Wick, P., 2014. How to consider engineered nanomaterials in major accident regulations? Environmental Sciences Europe 26, 1-10.
Oberdörster, G., Castranova, V., Asgharian, B., Sayre, P., 2015. Inhalation Exposure to Carbon Nanotubes (CNT) and Carbon Nanofibers (CNF): Methodology and Dosimetry. Journal of Toxicology and Environmental Health, Part B 18, 121-212. OECD, 2009. Compilation and Comparison of Guidelines Related to Exposure to Nanomaterials in Laboratories, ENV/JM/ MONO(2010)47, OECD, Paris.
Pattan, G., Kaul, G., 2014. Health hazards associated with nanomaterials. Toxicology and industrial health 30, 499-519.
Price, P., Stone, R., Collier, T., Davies, M., Scheer, V., 2006. Dynamic particulate measurements from a DISI vehicle: a comparison of DMS500, ELPI, CPC and PASS. SAE Technical Paper.
Sandberg, M., 1981. What is ventilation efficiency? Building and environment 16, 123-135.
Seipenbusch, M., Yu, Mingzhou, Asbach, Christof, Rating, Uwe, Kuhlbusch, Thomas A. J., Lidén, Göran, 2014. Chapter 4 - From Source to Dose: Emission, Transport, Aerosol Dynamics and Dose Assessment for Workplace Aerosol Exposure A2 - Vogel, Ulla, in: Savolainen, K., Wu, Q., Tongeren, M.v., Brouwer, D., Berges, M. (Eds.), Handbook of Nanosafety. Academic Press, San Diego, pp. 135-171.
Shepard, M., Brenner, S., 2014. Cutaneous exposure scenarios for engineered nanoparticles used in semiconductor fabrication: a preliminary investigation of workplace surface contamination. International journal of occupational and environmental health 20, 247-257.
Taurozzi, J.S., Hackley, V.A., Wiesner, M.R., 2012. Preparation of Nanoscale TiO2 Dispersions in an Environmental Matrix for Eco-Toxicological Assessment. NIST Special Publication 1200, 5.
Von der Weiden, S., Drewnick, F., Borrmann, S., 2009. Particle Loss Calculator–a new software tool for the assessment of the performance of aerosol inlet systems. Atmos. Meas. Tech 2, 479-494.
Walser, T., Hellweg, S., Juraske, R., Luechinger, N.A., Wang, J., Fierz, M., 2012. Exposure to engineered nanoparticles: model and measurements for accident situations in laboratories. Science of the total environment 420, 119-126.
Wang, J., Asbach, C., Fissan, H., Hülser, T., Kuhlbusch, T.A., Thompson, D., Pui, D.Y., 2011. How can nanobiotechnology oversight advance science and industry: examples from environmental, health, and safety studies of nanoparticles (nano-EHS). Journal of Nanoparticle Research 13, 1373-1387.
Whicker, J.J., Wasiolek, P.T., Tavani, R.A., 2002. Influence of room geometry and ventilation rate on airflow and aerosol dispersion: implications for worker protection. Health physics 82, 52-63.
Whitby, K.T., 1978. The physical characteristics of sulfur aerosols. Atmospheric Environment (1967) 12, 135-159.

Hinds, William, C. 1982. Aerosol technology. Properties, Behavior, and Measurement of Airborne Particles.

Zhong, K., Yang, X., Kang, Y., 2010. Effects of ventilation strategies and source locations on indoor particle deposition. Building and Environment 45, 655-662.